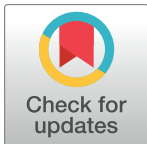# Zebrafish *snai2* mutants fail to phenocopy morphant phenotypes

Cara Bickers, Sophia D. Española, Stephanie Grainger, Claire Pouget, David Traver*

Department of Cellular and Molecular Medicine and Section of Cell and Developmental Biology, University of California, San Diego, La Jolla, CA, United States of America

* dtraver@ucsd.edu

Abstract

Snail2 is a zinc-finger transcription factor best known to repress expression of genes encoding cell adherence proteins to facilitate induction of the epithelial-to-mesenchymal transition. While this role has been best documented in the developmental migration of the neural crest and mesoderm, here we expand on previously reported preliminary findings that morpholino knock-down of *snai2* impairs the generation of hematopoietic stem cells (HSCs) during zebrafish development. We demonstrate that *snai2* morphants fail to initiate HSC specification and show defects in the somitic niche of migrating HSC precursors. These defects include a reduction in sclerotome markers as well as in the Notch ligands *dlc* and *dld*, which are known to be essential components of HSC specification. Accordingly, enforced expression of the Notch1-intracellular domain was capable of rescuing HSC specification in *snai2* morphants. To parallel our approach, we obtained two mutant alleles of *snai2*. In contrast to the morphants, homozygous mutant embryos displayed no defects in HSC specification or in sclerotome development, and mutant fish survive into adulthood. However, when these homozygous mutants were injected with *snai2* morpholino, HSCs were improperly specified. In summary, our morpholino data support a role for Snai2 in HSC development, whereas our mutant data suggest that Snai2 is dispensable for this process. Together, these findings further support the need for careful consideration of both morpholino and mutant phenotypes in studies of gene function.

Introduction

The small pool of hematopoietic stem cells (HSCs) derived during embryogenesis gives rise to the lifelong supply of all blood cells. HSCs are derived from the ventral wall of the dorsal aorta through a process referred to as the endothelial-to-hematopoietic transition (EHT)[1±6]. Before this event can occur, however, HSC precursors are directed by a complex cascade of signaling events. During development, both hematopoietic and endothelial precursors, which are derived from posterior lateral mesoderm (PLM), migrate beneath the somites to the embryonic midline to form the trunk vasculature[7,8]. During this migration, the somites provide instructional cues, including canonical Wnt[9] and Notch signaling[7,10,11], which culminate in specifying the cellular identity of hemogenic endothelium. Upstream of these signals, there is a complex network of other intrasomitic signaling events, including non-canonical Wnt and FGF signaling[10,12]. In addition, specific compartments of the somites, including the

sclerotome[10,11] and endotome[13], have also been identified as essential players in embryonic hematopoiesis. This is likely due to the compartmental specific relays required during the complex signaling cascade that forms the developmental HSC niche, a process that is incompletely understood. Further understanding of the niche will contribute to a major goal in regenerative medicine: reproducing the proper supportive environment for HSC instruction *in vitro*[14].

Using a genomics based approach, we previously identified *snai2* as upregulated in stromal cell lines supportive of HSCs *in vitro*[15]. The Snail family of zinc-finger transcriptional repressors includes three members: *snai1/snail*, *snai2/slug*, and *snai3/smuc*[16,17]. These repressors play critical roles during the epithelial-to-mesenchymal transition (EMT), and have been best studied in processes including gastrulation, neural crest delamination, and heart valve formation[18,19]. Snail2 has been shown to cell-intrinsically protect adult hematopoietic progenitor cells from radiation induced apoptosis[20], likely due to blocking self-renewal and proliferation [21]. $Snai2^{-/-}$ mice develop macrocytic anemia and impaired T-cell maturation; however, no defects in HSC specification, emergence, or differentiation have been reported[22]. In addition, redundancy of the Snail family in the hematopoietic system has been implicated, since the combined loss of Snai2 and Snai3, but not loss of either gene alone, leads to fatal lymphoid dysfunction[23,24].

To investigate *snai2* function in zebrafish, we used morpholino knock-down and mutant zebrafish alleles, where we identified inconsistencies between mutants predicted to have Snail2 loss of function and animals subjected to morpholino knock downÐa phenomenon also observed by groups targeting other genes[25±29]. Our knock down studies support a requirement for Snai2 in HSC development, upstream of Notch signaling, likely by promoting sclerotome formation. However, our mutant studies suggest that Snai2 is dispensable during HSC development, and that the Snai2 morpholino may have off-target or toxic effects. Overall, the discrepancies we observed between morpholinos and genetic mutants support the need to review and revise use guidelines for both morpholinos and mutants, as has been suggested by other groups[28,30].

Materials and methods

Zebrafish husbandry

Zebrafish were maintained and propagated as previously described[31], and this study was approved by the University of California at San Diego Institutional Animal Care and Use Committee (UCSD IACUC) under protocol number S04168. Embryos and adult fish were raised in a circulating aquarium system (Aquaneering) at 28ÊC. All anesthesia was completed with 100 mg/L Tricaine solution, and euthanasia of adult fish was completed with an ice slurry. The following zebrafish strains were used: wildtype AB*, *Tg(CD41:GFP)*[32], *Tg(kdrl:mCherry)* [33], *Tg(Gata2b:Gal4/UAS:LA-GFP)*[34], *Tg(actc1b:GFP)*[35], $Tg(TP1:GFP)^{um14}$ [36], *Tg (5xUAE-E1b:6xMYC-notch1a)^{kca3}* [37] referred to as *Tg(UAS:NICD-myc)* for simplification, *Tg (kdrl:miniGal4)*[11], $snai2^{sa24539}$ [38], $snai2^{112\Delta}$, and $p53^{-/-}$ [39]. The deletion mutant of *snai2* was produced utilizing the CRISPR/Cas9 genomic editing system. gRNAs were designed utilizing the CHOP-CHOP web-tool and coninjected with Cas9 mRNA, as previously described [40±42]. gRNAs were designed to target three sequences within the *snai2* gene: `CCTCAGCCTG AAGTGTTAAGCCC`, `CCCCTTCCCCACGACCTGTCCCC`, and `CCTCATCTCTCTCTGACACA TCC`. A 112 base pair deletion, predicted to result in frame-shift and early termination was isolated and propagated for studies. The allele number of this mutant is #SD57.

Whole mount *in situ* hybridization (WISH) and histology

WISH and double fluorescent WISH were conducted as previously described[12,43], using established DIG-labelled or fluorescein labelled anti-sense RNA probes including *runx1*, *foxc1b*, *dlc*, *dld*, *cmyb*, *gata1*, *fli1a*, *kdrl*, *dll4*, *cdh17*, *rag1*, and *jam2*[7,10]. Antisense probes for *snai2*, *snai1a*, *snai1b*, and *pax9* were designed to target the entire coding region. Following WISH, selected embryos were processed for cryosectioning, according to standard procedures on the Leica CM1860 Cryostat at 10 μm thickness. WISH and Cryosections were imaged on a DFC295 digital camera using the Leica FireCam Software. All confocal images of double fluorescent *in situ* hybridization and fluorescent transgenic embryos were obtained with a Leica SP5 inverted confocal microscope (Leica Microsystems).

Microinjections of mRNA and morpholino

Embryos were injected at the one-cell stage with morpholino oligonucleotides (MOs, Gene-Tools) and/or mRNA. Antisense MOs were used at the following concentrations: 10 ng *snai2* splice-block MO (SB MO)[15,44] and 0.75 ng *snai2* 5'UTR MO (UTR MO). Capped mRNA was synthesized from linearized pCS2$^+$ constructs using the mMessage mMachine SP6 Transcription Kit (ambion, AM1340), according to manufacturer's recommendations. Full length *snai2* mRNA was injected into embryos at 150 ng/μl.

Cell Sorting and real-time quantitative PCR (qPCR)

Double transgenic *Tg(CD41:GFP/kdrl:mCherry)* or *Tg(actc1b:GFP)* embryos were prepared for flow cytometry at 48 hpf and 17 hpf, respectively as previously described[45]. Single, live cells were sorted on a FACSAria II and collected for RNA extraction. Total RNA was extracted from pools of embryos via TRIzol (Ambion) and sorted cells using the RNEasy Mini Kit (Qiagen, 74104), cDNA was synthesized using iScript gDNA Clear cDNA Synthesis Kit (Bio-Rad), and RT-qPCR reactions were performed using SYBR Green (Bio-Rad) and a Bio-Rad CFX96 real time system according to the manufacturer's instructions. The expression of housekeeping genes *ef1α* and *β-Actin* were used to normalize using the $\Delta\Delta C_t$ method. Primer sequences are listed in Table 1.

Immunohistochemistry (IHC)

NICD expression was confirmed using immunohistochemistry was completed with anti-c-myc antibody (1:1000, BioLegend) post-WISH, as previously reported[46]. Embryos were imaged for GFP fluorescence on the AxioZoom.V16 (Zeiss), followed by brightfield imaging on the Leica MZ16.

Snai2^{112Δ} and *Snai2^{sa24539}* genotyping

Snai2^{112Δ} were generated as described above and genotyped using the following primers: forward 5′–ATGTGACCTGTCAAAGTATGGC–3′ and reverse 5′– TACACAAACCGCACTGA AACTT–3′. Zebrafish embryos with a nonsense point mutation in the second exon of *snai2* were obtained from the Zebrafish International Resource Center (ZIRC)[38]. The single nucleotide polymorphism (SNP) specific genotyping primers, designed as previously described[47], used are as follows: forward 5′– CACATCCTCTAATAAGGACCACAGCGGT–3′ and reverse 5′– GCTTCATGAGTCCCGAATACGTGTTG–3′.

Table 1. qPCR primers.

Gene	Forward	Reverse
ßactin	cgtctggatctagctggtcgtga	caatttctctttcggctgtggtg
cmyb	agagggtgaaagaaatcgag	actgaaacaacaatgccaac
dlc	acgagcagtgtgtgtaa	tgttattctctgttgactgg
dld	agtactgcacagaacc	tcttggttacagaagag
ef1a	gagaagttcgagaaggaagc	cgtagtatttgctggtctcg
kdrl	ctcctgtacagcaaggaatg	atctttgggcaccttatagc
meox	ggcttttaccaaagagcaac	tttgaaaccacactttcacc
snai1a	tgaagatgcacatccgctc	gttacagtgtgggcaggag
snai1b	tatccctccatgcttgtgtg	tcatcctcctctccactgct
snai2	accgaattatagtgaactggaga	actgttatgggattgtacgcc
snai3	cacacaggtgagaaaccatt	ttgatctcagagtgggtttg
twist1b	aatcatccccactttaccttc	gtgagcaacataactacaactt

Whole kidney marrow analysis

Zebrafish kidneys were prepared for flow cytometry as previously described[48] and resuspended in 1x PBS with 1% fetal bovine serum. Samples were analyzed on a BD LSR II Flow Cytometer to separate cellular fractions by size and granularity as previously described[49].

Results

Snai2 is expressed in the embryonic hematopoietic niche

To explore the role of Snail2 in embryonic hematopoiesis, its expression pattern was observed via whole-mount *in situ* hybridization (WISH) throughout early development. At 14 hours post fertilization (hpf), when the PLM has not yet begun its migration to the midline, *snai2* is highly expressed in the nervous system, somites, and an outer stripe of the mesoderm (Fig 1A). This expression pattern continues throughout somitogenesis, with somitic expression becoming localized to the most ventral portion of the somites (Fig 1B±1G), the tissue that most closely contacts migrating HSC precursors. At both 14 hpf (pre-migration) and 24 hpf (post-migration), *snai2* transcript showed no colocalization with the endothelial markers *fli1a* or *etsrp* via double fluorescent *in situ* hybridization (Fig 1H and 1I). QPCR from FACS purified hematopoietic stem and progenitor cells (HSPCs) and endothelial cells at 48 hpf demonstrated that *snai2* was not enriched in either population, as compared to all other cells in the embryo (Figs 1I and S1), suggesting that Snai2 function is not required cell-intrinsically.

Snai2 Morpholinos lead to a depletion of HSPCs

We confirmed splicing defects using a previously reported splice blocking (SB) morpholino targeting the exon2-intron2 junction (Figs 2A and S1). The resulting misspliced gene product was sequenced to predict the amino acid sequence and protein structure, which indicated that the SB transcript should produce a protein truncated just beyond the first zinc finger (Fig 2B and 2C)[15,44]. The loss of the majority of the zinc-finger domains is expected to prevent DNA binding, and protein function. WISH for *runx1*, a marker of HSC commitment, indicated a decrease of HSCs in the dorsal aorta at 26 hpf, which could be rescued using an exogenous, SB-resistant *snai2* mRNA (Fig 3A). *Snai2* mRNA injected alone was not seen to affect expression of *runx1*. Furthermore, by 48 hpf, there was also a significant decrease of HSCs in
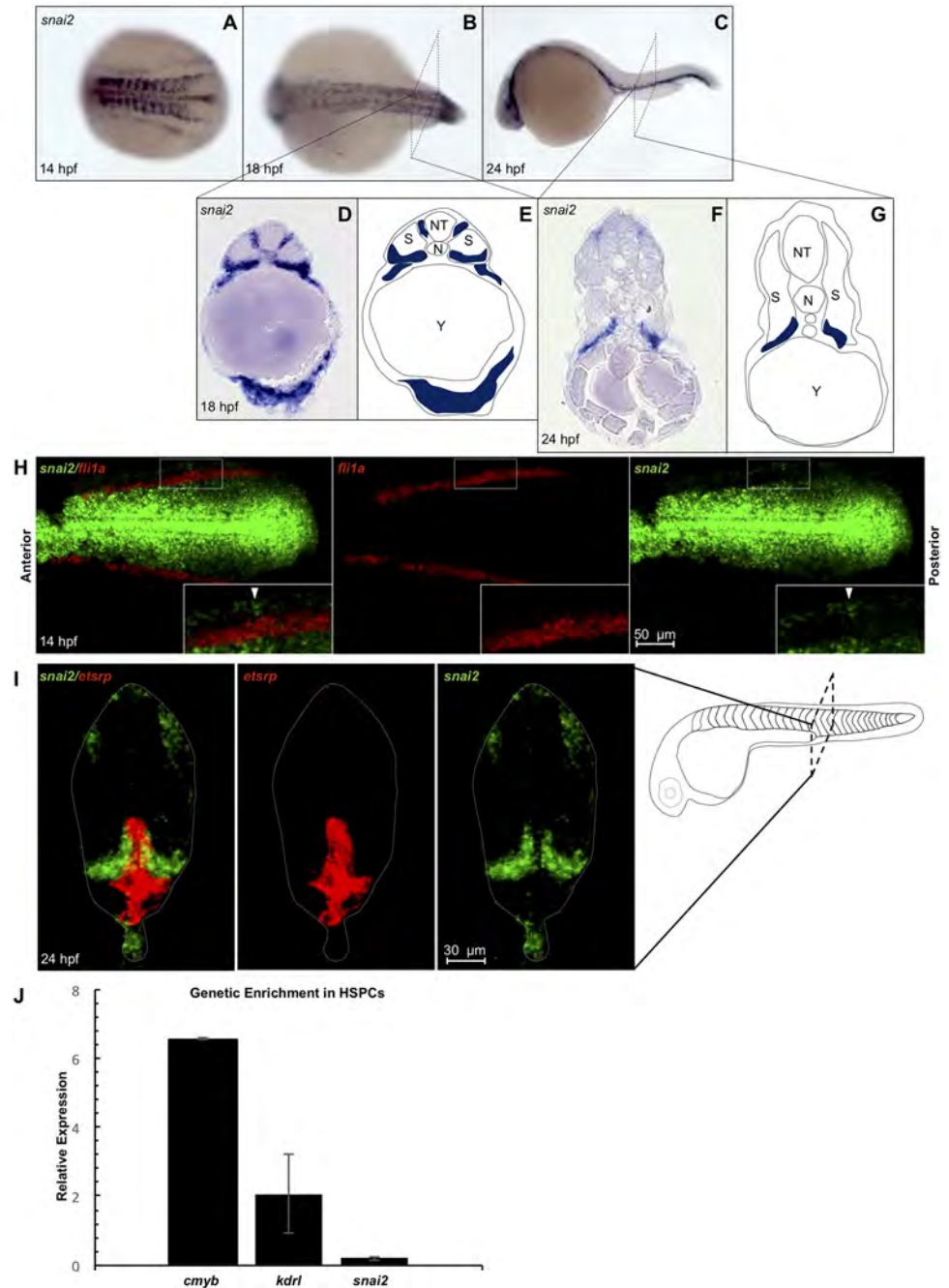
Fig 1. *Snai2* endogenous expression in wild-type embryos. Expression of *snai2* was analyzed via whole mount *in situ* hybridization at 14 hpf (A), 18 hpf (B), and 24 hpf (C). Embryos were cryosectioned post-*in situ* at 18 hpf (D) and 24 hpf (F). Simplified schematics are provided (E and G). Double fluorescent *in situ* for *snai2* with endothelial markers *fli1a* at 14 hpf (H) and *etsrp* at 26 hpf (I) was performed. Insets show a close-up view of the PLM. QPCR was used to compare *snai2* enrichment within double positive HSPCs sorted from *Tg(CD41:GFP/kdrl:mCherry)* on 2 dpf to the rest of the embryo. Markers *cmyb* and *kdrl*, which should be enriched in this population, are displayed alongside for comparison. N: notochord; NT: neural tube; S: somite.

the SB morphants, as assessed by confocal imaging of *gata2b* reporter embryos (Fig 3B and 3C).
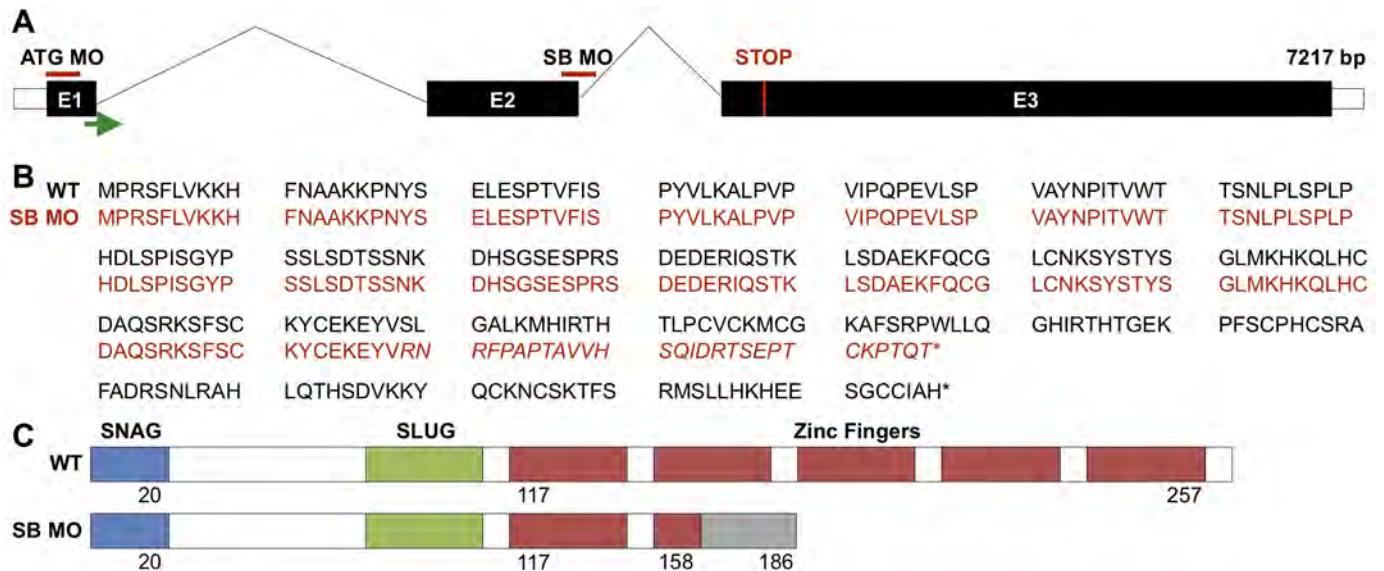
Fig 2. Predicted genomic and protein effects of *snai2* morpholinos. Location of the splice-blocking and translation-blocking morpholinos are indicated on a schematic of the *snai2* gene (A). The green arrow indicates the transcription start site, and the red line the endogenous stop codon. Predicted effects on the amino acid sequence (B) and protein structure (C) are shown for wild-type and SB morphant fish. 121 bp of exon 2 are lost due to the aberrant splicing event, leading to a truncation of the protein within the zinc-finger domain. Italicism of the amino acid sequence and the grey region of the structure indicate a region of missense amino acids prior to the early stop codon. E: exon; SB: splice-block; MO: morpholino.

The requirement for Snai2 in the derivation of endothelial cells was assessed using WISH for markers of the PLM (*fli1a*; S2 Fig) and the trunk vasculature (*fli1a*, *kdrl*; S2 Fig), which were normal. Primitive hematopoiesis appeared normal (*gata1*; S3 Fig). Additionally, the formation of the pronephros, which will develop into the adult hematopoietic niche, appeared normal (*cdh17*; S3 Fig).

These results were recapitulated using a translation blocking (ATG) morpholino (Fig 2A), which also resulted in a decrease in HSC specification at 26 hpf (Fig 3A). ATG morphants had a similar decrease in emerging HSPCs in Tg-HSC animals (S4 Fig). Levels of the hematopoietic marker *cmyb* in the caudal hematopoietic tissue at 48 hpf were also reduced, as previously reported in the SB morphants (S4 Fig). Taken together with the mRNA rescue and SB morpholino data, these results suggest that both morpholinos specifically target *snai2*. We completed our further studies using the SB morpholino alone.

Snai2 Morphants display sclerotome defects

The combined observations of loss of early HSC specification in *snai2* morphants and high *snai2* expression in the ventral somites suggested that Snai2 may function in the sclerotome, which is known to be involved in HSC specification[10,11]. Indeed, *snai2* morphants lacked *pax9* (sclerotome marker) staining in their posterior somites, though *pax9* expression was unaffected in the most anterior somites (Fig 4A). Morphants also displayed a decrease in *twist1b* (sclerotome marker) transcripts by qPCR in sorted somitic cells, whereas levels of *meox* (pan-somitic marker) were unaffected (Fig 4B). This suggested that the sclerotome compartment of posterior somites is specifically affected by loss of *snai2*. Supporting this, the structure of the sclerotome was disrupted in SB MO embryos, as assessed by *foxc1b* (Fig 4C and 4D), while *myoD* (myogenic marker) expression was induced normally (Fig 4D), further supporting the specificity of Snai2 function. Altogether, these analyses indicate that *snai2*
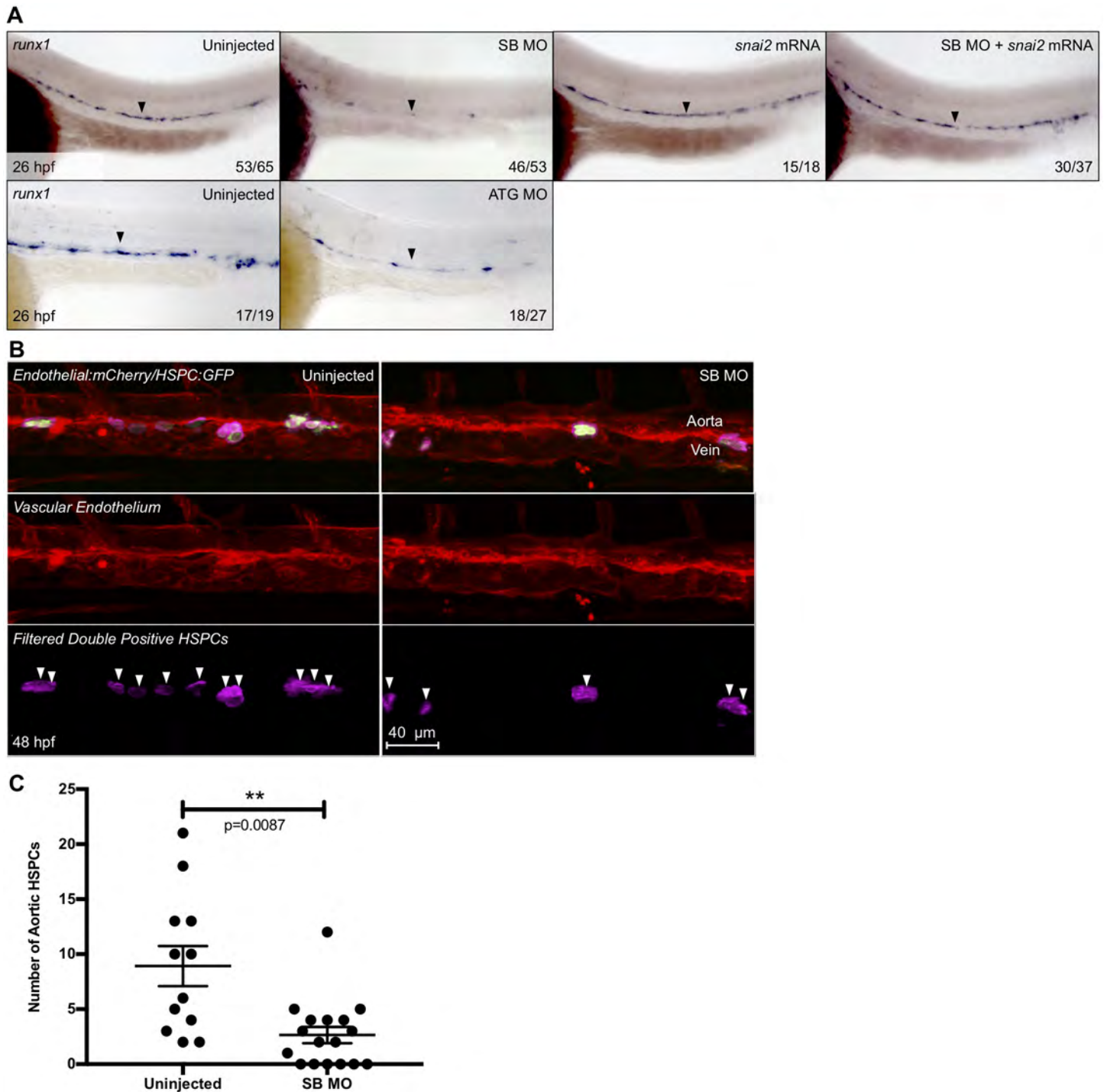
Fig 3. Snai2 morphants display a strong defect in HSC specification. Expression of the HSC specification marker, *runx1*, was analyzed by *in situ* hybridization at ~26 hpf in embryos injected with SB MO, ATG MO, and their siblings (A). The effect of *snai2* mRNA injection was also analyzed both alone and when coinjected with SB MO. Black arrowheads point to the middle of the aortic *runx1* expression. Numbers in the lower right hand corner of each image depict the number of embryos with the phenotype pictured out of the total number of embryos assayed in each condition. *Tg(gata2b:Gal4/UAS:LA-GFP/kdrl:mCherry)* morphants and their siblings were imaged by confocal microscopy at 48 hpf, and Imaris imaging software was used to remove GFP signal outside of the vasculature (B). Pink coloration is indicative of double positive cells as filtered by the surfaces feature of Imaris. White arrowheads indicate separate putative HSPCs. Quantification for each fish was graphed and statistically analyzed by non-parametric *t*-test on Prism (C). Error bars are SEM.
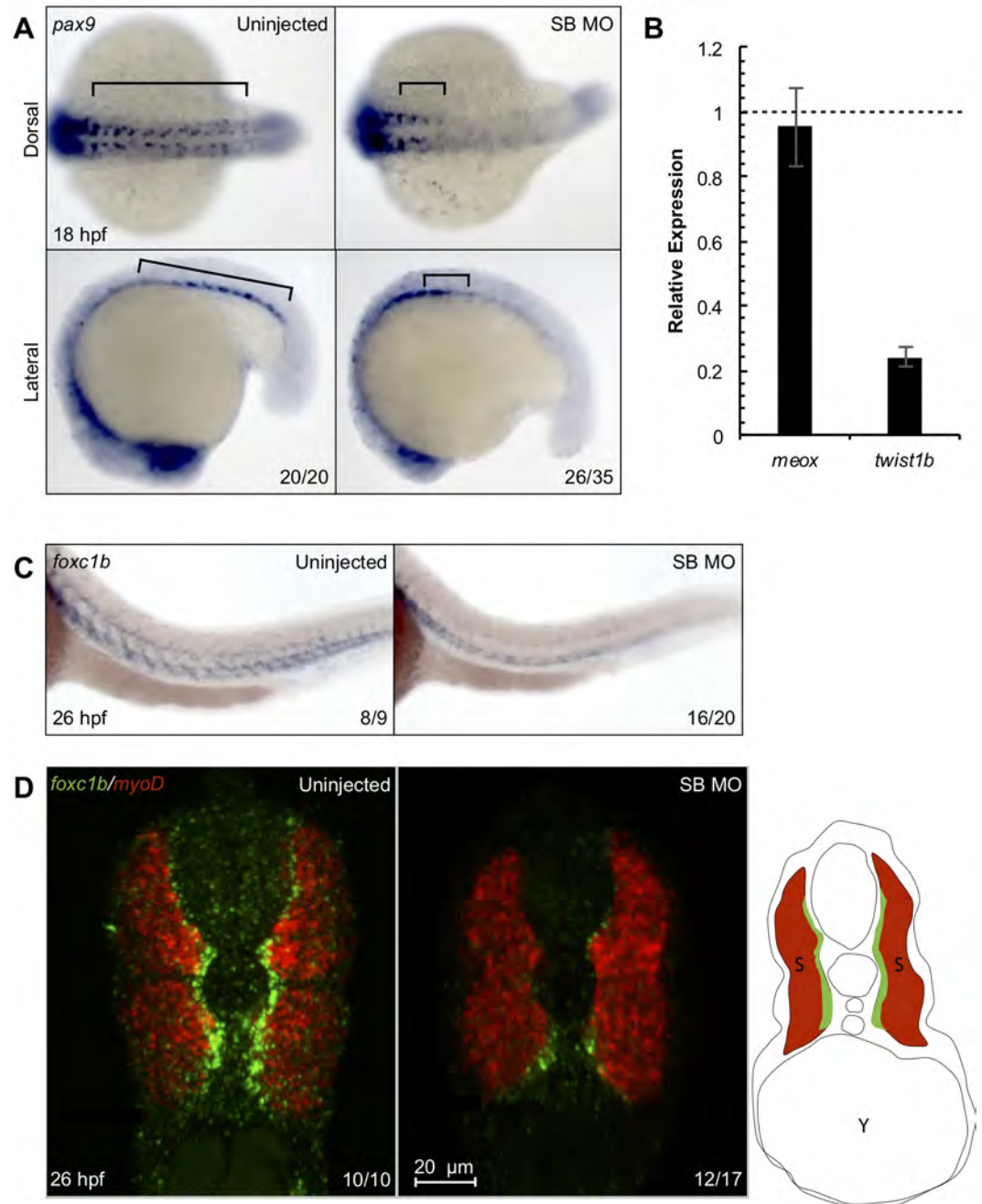
https://doi.org/10.1371/journal.pone.0202747.g003

Fig 4. *Snai2* SB morphants display depletion of sclerotome markers. *pax9*, a marker of the sclerotome, was analyzed by WISH at 18 hpf (A). Black brackets highlight the difference in staining between morphants and siblings. qPCR on somitic, GFP+ cells sorted from morphant and control *Tg(actc1b:GFP)* embryos at ~17 hpf showed the sclerotome marker *twist1b* was decreased, while the pan-somitic marker remained normal in morphants (B). Wish for *foxc1b* showed clear diagonal expression in the anterior portion of the somites of uninjected embryos, while morphants lacked this distinctive stripe pattern (C). Error bars are calculated from technical replicates. Double fluorescent *in situ* hybridization for *foxc1b and myoD* (myogenic marker) followed by razor cutting for confocal analysis showed that while the muscle marker is consistent in both morphants and uninjected embryos, there is a notable decrease of positive staining for *foxc1b*, especially within the dorsal portion of the somites. A small schematic is provided to show greater detail of how embryos are oriented in Fig D. Numbers in the lower right-hand corner of each image depict the number of embryos with the phenotype pictured out of the total number of embryos assayed in each condition.

https://doi.org/10.1371/journal.pone.0202747.g004

morphants have a defect in sclerotome formation that could directly affect the downstream specification and maintenance of HSCs.

Snai2 morphants display defective Notch signaling

Notch signaling plays multiple essential roles in the specification of the HSC[50], and the ventral somites have been shown to be one source of this activity[7], which ultimately culminates in aortic Notch signaling during HSC emergence. Utilizing a transgenic Notch-activity reporter we determined that 26 hpf morphants lacked aortic Notch activity (Fig 5A and 5B). However, aortic identity was partially spared, as morphants had normal levels of aortic *dll4* and *dlc* (S5 Fig). This suggests that loss of *snai2* leads to loss of aortic Notch activity and HSCs. Indeed, endothelial-specific expression of the Notch1 intracellular domain was able to rescue loss of HSCs in *snai2* morphants (Figs 5C and S5), suggesting that Notch signaling lies downstream of Snai2 function.

The data above suggested that *snai2* deficient somites may be defective in Notch ligand production. In this regard, morphants were deficient for *dlc* and *dld* in the anterior somites (Fig 5D). These results were confirmed by qPCR on somitic cells (Fig 5E) and double fluorescent *in situ* for *dld* and *myoD* (S5 Fig). The SB morphants also have normal expression of the adherence protein *jam2a*, indicating that although Notch ligands are not presented properly from the somites, this tissue is still capable of closely interacting with the migrating PLM[7] (S5 Fig). Altogether, these data suggest that somitic *snai2* is required for *dlc* and *dld* expression, which is necessary for downstream Notch activity in HSC precursors.

Generation of a Snail2 mutant zebrafish

To test the effect of total Snail2 loss of function, we generated a mutant using CRISPR/Cas9 to induce a mutation in the second exon of the gene (Fig 6A). This mutation was analyzed by sequencing the resulting transcript. The zebrafish line possessed a 112 base pair deletion in the coding region, which is predicted to cause a frameshift, early stop codon, and truncated protein (Fig 6B). This deletion is easily detectable by PCR (S6 Fig). The truncated protein is predicted to lack function due to the loss of the SLUG recruitment domain and all DNA binding motifs (Fig 6C). We also obtained an ENU-derived mutant predicted to cause a truncated protein lacking most of the zinc finger domains (Fig 6A±6C).

Snai2$^{112\Delta/112\Delta}$ and snai2 $^{sa24539/sa24539}$ do not display defects in HSC specification or sclerotome formation

In contrast to morphants, there was no difference in the early specification marker *runx1* or the later hematopoietic marker *cmyb* in either *snai2*$^{112\Delta/112\Delta}$ or *snai2* $^{sa24539/sa24539}$ embryos (Fig 7A and 7B). The mutants also showed normal levels of the T-cell marker *rag1* (S6 Fig), suggesting normal embryonic HSPC differentiation capacity. Additionally, sclerotome formation was normal in both mutant lines, as assayed by expression of *foxc1b* (Fig 7C). Finally, there was no significant difference in emerging HSCs in Tg-HSC animals harboring the *snai2*$^{112\Delta/112\Delta}$ mutation (Fig 7D and 7E). Altogether, these results indicated that embryonic hematopoiesis was normal in both *snai2* mutants.

Snai2$^{112\Delta}$ mutants survive to adulthood with healthy whole kidney marrow

The zebrafish kidney is the site of adult hematopoiesis, akin to mammalian bone marrow. Different cellular fractions were assayed by flow cytometry for size and granularity, where we found that wildtype, heterozygotes, and morphants had statistically similar cellular distributions,
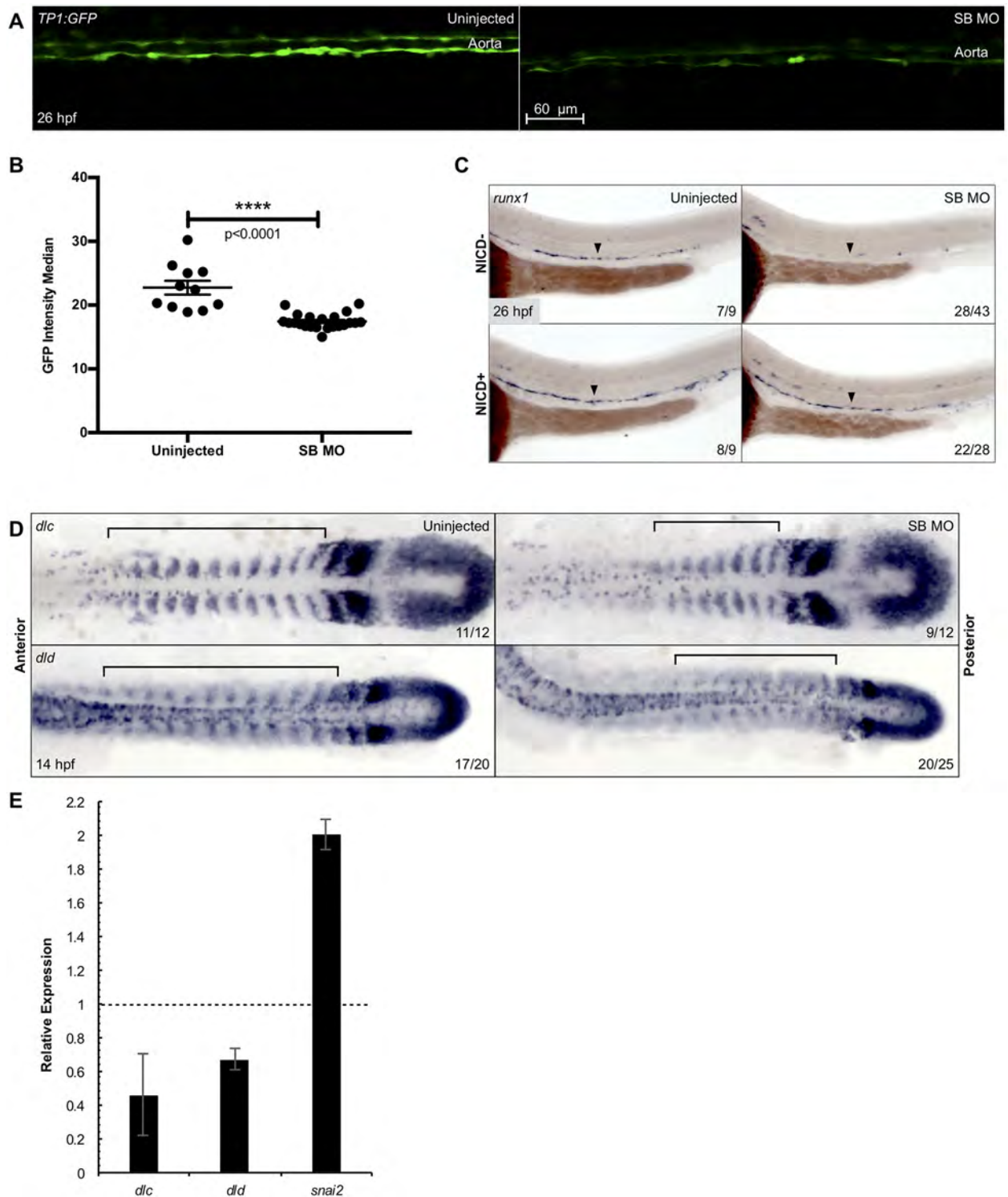
Fig 5. *Snai2* SB morphants have defective Notch signaling. Aortic Notch activity was assessed by confocal microscopy of the Notch reporter *Tg (TP1:GFP)* (A). Median fluorescence intensity was calculated by the surfaces feature of Imaris and was graphed and statistically analyzed by a non-parametric *t*-test on Prism (B). Error bars are SEM. Using a combination of *Tg(kdrl:miniGal4)* and *Tg(UAS:NICD-myc)*, we saw that ectopically activating Notch signaling within the endothelium was sufficient to rescue expression of the HSC marker *runx1* in morphant embryos (C). Black arrowheads point to the middle of the aortic *runx1* expression. Analysis by WISH displays that expression of the Notch ligands *dlc* and *dld* is decreased in morphants, especially within the more anterior somites (D). Black brackets are provided to highlight the differences in staining. This decrease was further confirmed by qPCR in somitic, GFP+ cells sorted from morphant *Tg(actc1b:GFP)* embryos as compared to uninjected siblings

(E). *Snai2* relative expression is included for comparison, since the misspliced transcript is consistently elevated in SB MO injected embryos. Error bars are calculated from technical replicates. Numbers in the lower right-hand corner of each image depict the number of embryos with the phenotype pictured out of the total number of embryos assayed in each condition.

consistent with a lack of defects in embryonic hematopoiesis (Fig 8A and 8B). However, there is a slight trend towards less erythroid and lymphoid cells within the mutants, similar to the defects found in adult *snai2* mutant mice, which may suggest that this function is conserved. These mutant adults are also capable of breeding and producing healthy, viable progeny who grow to adulthood without incident.

Probing morphant vs. mutant phenotype validity

Since recent studies have shown that permanent genomic disruption of a gene can lead to enhanced expression of similar genes[51], we examined the expression of all members of the Snail transcription factor family. WISH for both zebrafish orthologues of *snai1* at the time of PLM migration onset showed similar levels of expression in wildtype, heterozygous, and mutant embryos (Fig 9A). However, at 26 hpf, qPCR displayed a 1.5- to 2-fold increase of *snai1a*, *snai1b*, and *snai3* in the mutants (Fig 9B), suggesting some functional compensation may occur.
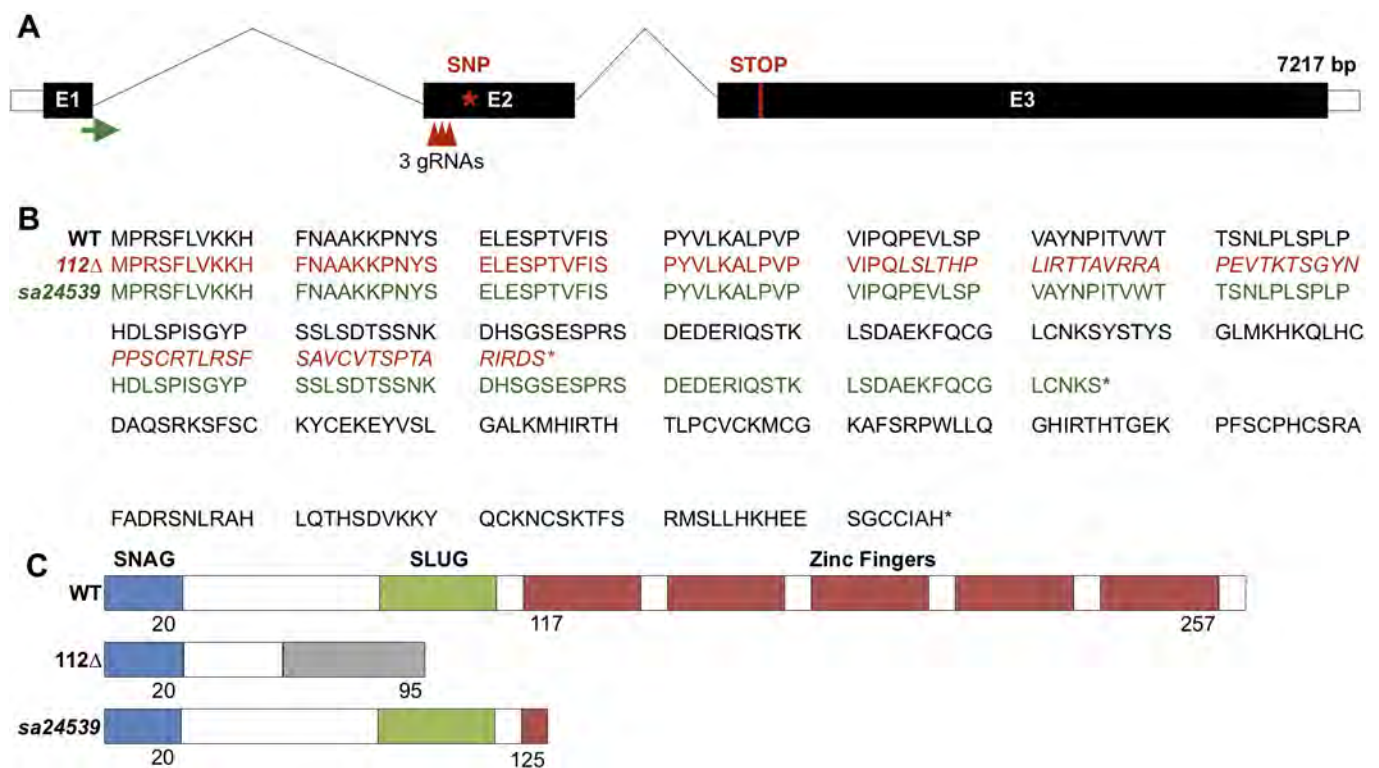

Fig 6. Predicted genomic and protein effects of the mutant *snai2* alleles. A schematic of the *snai2* gene displays where the three guide RNAs (gRNAs) were designed for CRISPR/Cas9 directed mutagenesis (red arrowheads) as well as the single nucleotide polymorphism (SNP) location in the mutagenesis derived *snai2*^sa24539 allele (red *) (A). The endogenous stop codon is indicated by the red line in exon 3. Predicted effects on the amino acid sequence (B) and protein structure (C) of wild-type, *snai2*^112Δ, and *snai2*^sa24539 are depicted. For the *snai2*^112Δ allele, a 112 bp deletion within the beginning of exon 2 leads to a truncation prior to the zinc-finger domain. Italicism of the amino acid sequence and the grey region of the structure indicate a region of missense amino acids prior to the early stop codon. The *snai2*^sa24539 allele SNP is a stop codon.
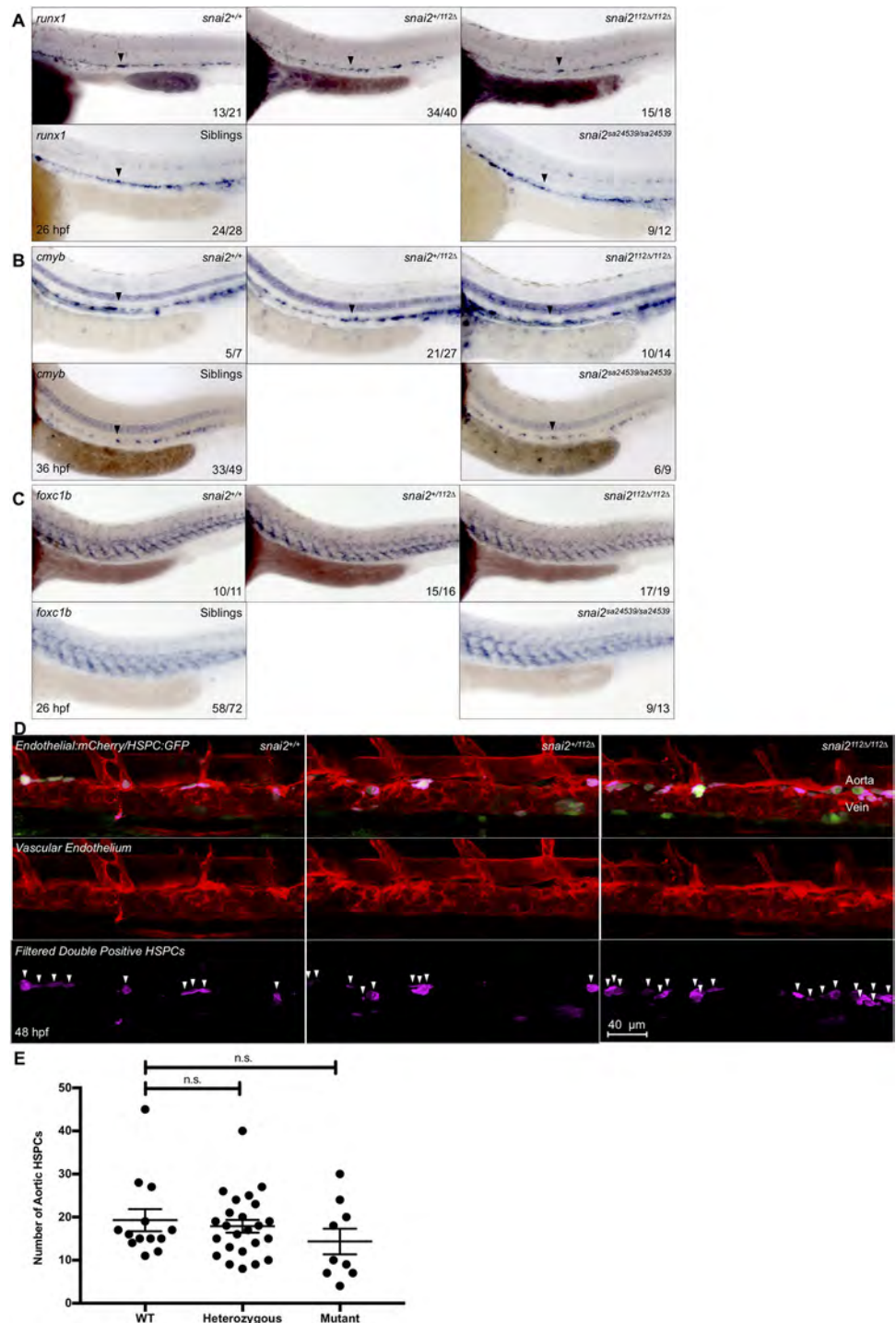
Fig 7. Snai2^{112Δ} and snai2^{sa24539} mutants have no embryonic defects in HSC or sclerotome formation. WISH analysis was performed on embryos derived from heterozygote in-crosses including probing for the hematopoietic markers *runx1* (A) and *cmyb* (B) and the sclerotome marker *foxc1b* (C). Wild-type, heterozygotes, and mutants are all included for the *Snai2^{112Δ}* allele since genotyping without sequencing was possible. For the *snai2^{sa24539}* allele, genotyping by PCR was sufficient to determine which embryos lacked the wild-type SNP, but not to distinguish wild-type from heterozygote. Thus, images are included for mutants versus ᵃsiblingsᵒ. For all markers, no obvious defect is detected. Black arrowheads point to the middle of the aortic *runx1* or *cmyb* expression. Numbers in the lower right-hand corner of each image depict the number of embryos with the phenotype pictured out of the total number of embryos assayed in each condition. HSC specification was also analyzed in *Tg(CD41:GFP/kdrl:mCherry)* fish on the

snai2[112Δ] background by confocal microscopy at 48 hpf, and Imaris imaging software was used to remove GFP signal outside of the vasculature (D). Pink coloration is indicative of double positive cells as filtered by the surfaces feature of Imaris. White arrowheads indicate separate putative HSPCs, and quantification for each fish was graphed and statistically analyzed by a non-parametric *t*-test on Prism (E). Error bars are SEM.

https://doi.org/10.1371/journal.pone.0202747.g007

On the other hand, it has also been shown that some morpholinos have either off target or toxic effects on embryonic development that can masquerade as specific phenotypes. Therefore, we assayed whether injection of the SB MO was capable of causing a reduction in HSC specification in an embryo with only mutant *snai2*. Indeed, decreases in both *runx1* by WISH (Fig 9C) and in HSC emergence in a transgenic reporter line (Figs 9D and S6) were shown across all genotypes. *Snai2* ATG MO also decreased *runx1* expression across all genotypes (S6 Fig). Some morpholinos are known to cause phenotypes due to an increase in *p53* transcript [52]; however, qPCR on 26 hpf embryos showed only slight elevation, and *p53* mutation did not affect the number of HSPCs in SB morphants (S7 Fig).

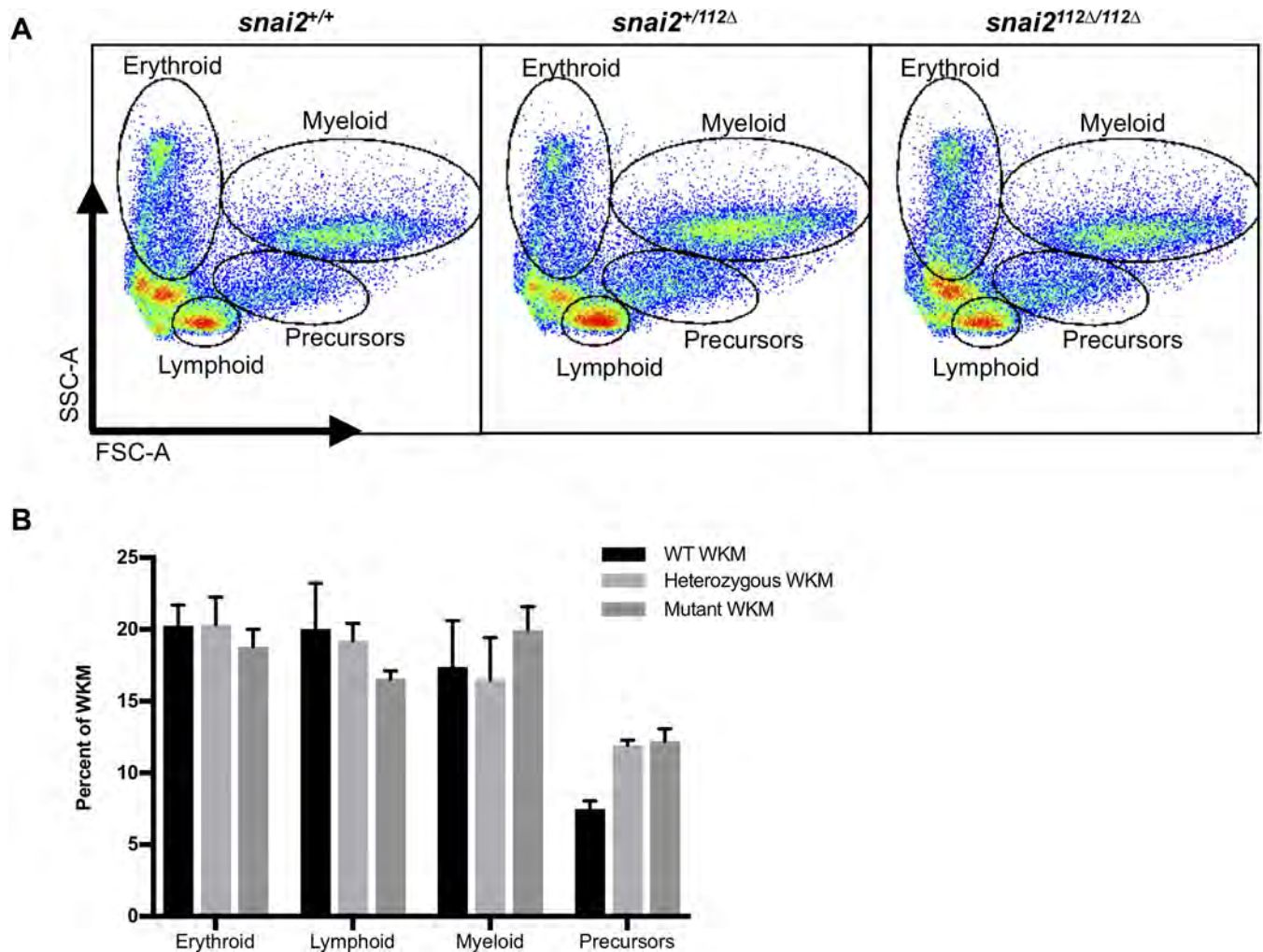**Fig 8. *Snai2*[112Δ] mutant adult hematopoiesis appears normal.** We analyzed the adult whole-kidney marrow (WKM) of 6-month-old *Snai2*[112Δ] mutants and their siblings by flow cytometry. Analyzing the cells by forward and side-scatter (A) displayed no significant difference between the various hematopoietic populations via two-way ANOVA (B). Error bars are SEM.
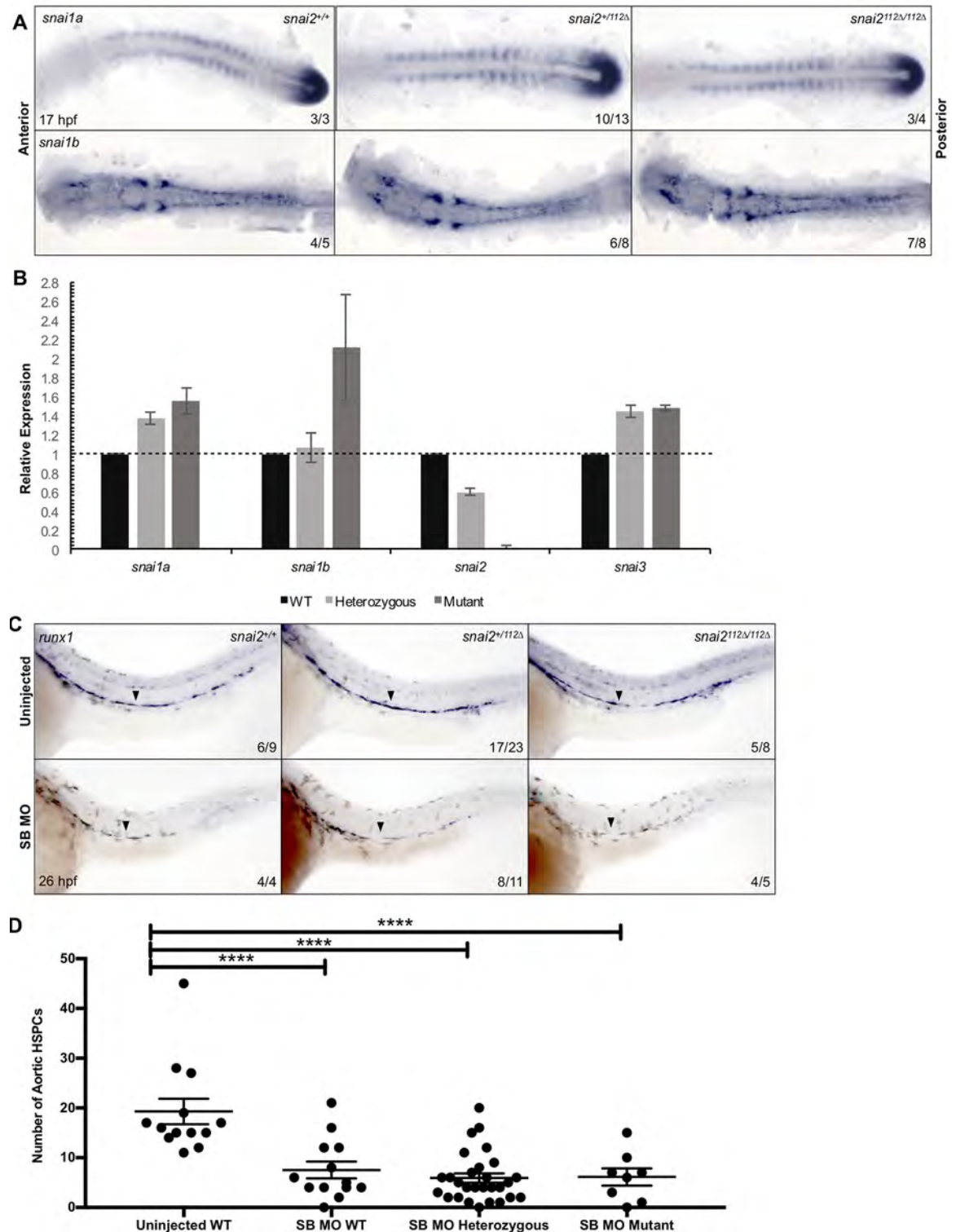
https://doi.org/10.1371/journal.pone.0202747.g008

Fig 9. Preliminary investigation of morphant vs. mutant phenotype. WISH within 17 hpf embryos from an in-cross of *snai2+/112Δ* displayed that the Snail family members *snai1a* and *snai1b* are not differentially expressed in mutant embryos as compared to heterozygote and wild-type siblings (A). However, qPCR in pooled embryonic trunks at 26 hpf showed a different trend: all 3 additional members of the Snail family show increased expression (B). This graph presents the average of two independent experiments in which embryonic heads were removed and genotyped, followed by pooling of trunks of the same genotype. Error bars are SD. *Snai2* reverse primer is designed within the mutant deletion, so transcript decrease reflects present of mutant transcript. We also observed the effect on

emerging HSCs when the SB MO was injected into mutant embryos and their siblings by observing both WISH for *runx1* at 26 hpf (C), and the double positive population in *Tg(CD41:GFP/kdrl:mCherry)* embryos at 48 hpf. Double positive cells were filtered by the surfaces function on Imaris, quantified, and submitted to statistical testing by a non-parametric *t*-test on Prism (D). Error bars are SEM. By both analyses, HSC specification was affected by SB MO in all genetic backgrounds. Black arrowheads point to the middle of the aortic *runx1* expression. **** represents $p < 0.0001$. WT: Wild-type.

Discussion

In this study, we more closely analyzed the hematopoietic phenotype previously identified in *snai2* morphant zebrafish embryos and characterized two mutant zebrafish *snai2* alleles. Previously published data from *snai2* morphants had suggested that Snail2 plays a role in the etiology of HSCs, and our data from two independent morpholinos supported this. Additionally, we were able to rescue this HSC specification defect with *snai2* mRNA, indicating that the MO effect is specific. *Snai2* transcripts were highly expressed in the somites, a tissue known to be intimately involved in specification of the HSC. Furthermore, *snai2* morphants displayed defects in markers of the sclerotome and significant decreases of the somitic Notch ligands *dlc* and *dld*. Both of these defects are known to lead to problems with HSC formation, and in these morphants, *snai2* may play an upstream role in both sclerotome formation and Notch signaling. However, in two independent mutants of the *snai2* locus, we did not observe any significant defects in hematopoiesis. Indeed, *snai2^{112Δ}* mutants are capable of interbreeding and producing progeny that grow and thrive normally, indicating that maternal deposition of *snai2* transcript does not play a role in rescuing the mutant phenotype.

This discrepancy between morphant and mutant phenotype is a problem on the rise in zebrafish research. Multiple recent studies have described similar results focused on a variety of different genes ([25±29]), and there has been great debate on the topic of morpholino use. From one perspective, it seems that the potential off target or toxic effects of these oligonucleotides outweighs their utility as a tool for genetic knockdown; however, an in depth study has also shown that deleterious mutations can induce complex genetic compensation that can obscure the role of a factor in a given process[51]. In that case, a finely tuned knockdown of gene expression allows us to decipher a factor's role, while a knockout may induce too much genetic compensation to deconvolute this. Both possibilities must be equally weighed, and great care must be taken when characterizing both new morpholinos and mutant alleles. New guidelines are now emerging to help deal with this growing issue[30]; however, the reality is that there are endless studies that now should be revisited to further asses genetic function.

The *snai2* morpholinos were capable of inducing a defect in HSC specification in the *snai2^{112Δ}* mutant, which strongly argues that the morpholino has an effect on either overall toxicity, or affects a target other than *snai2*, assuming the mutant does indeed cause loss of function. Additionally, while analysis of the *snai2* null mouse had shown a variety of effects on adult hematopoiesis, no defect in HSC specification or emergence has been identified. Finally, the increase of *p53* transcripts seen in the *snai2* SB morphants could indicate a problem with overall toxicity.

On the other hand, we present strong data that the morpholino knockdown of *snai2* is specific. The effect on HSC formation is specific: mRNA overexpression is capable of rescuing the *runx1* phenotype, and the second morpholino phenocopies the first. The overall development of morphant embryos is minimally affected, and structures including the aorta, cardinal vein, pronephros and most of the somite are unaffected. Finally, the Notch deficiency seen in the *snai2* morphants, is rescuable by overexpression of NICD in the vascular endothelium, again indicating a specific effect.

In further support of the morphant phenotype, the *snai2*$^{112\Delta}$ mutants show elevated *snai1a*, *snai1b*, and *snai3* transcripts, which could indicate some level of genetic compensation, and that one of the other factors could be taking on the role of *snai2* when absent. It is also formally possible that there are unknown factors compensating for this genetic loss of function. Further testing within the mutant would be essential to determine whether or not this is the case, including a much deeper probing of the mutant exome. It would also be interesting to create stable mutant forms of the other Snail family members, and then cross them appropriately to the Snail2 mutant fish. Previous studies have shown genetic redundancy by such an approach when a morpholino and mutant phenotype did not agree[53]. We performed a preliminary test of this redundancy by injecting *snai1a* morpholino into the *snai2*$^{112\Delta}$ mutants and their siblings; however, *runx1* expression was not strongly affected(S6 Fig). It may be the case that a second factor is still providing compensation, or that Snail1a in particular does not function redundantly with Snail2.

Another possibility is that these mutant alleles do not generate a true loss of function. The effects on protein translation can be predicted *in silico*; however, due to the absence of a zebrafish specific antibody to Snail2, it is impossible to know if these animals have generated a partially functional truncated protein, perhaps due to an alternative start site downstream of these mutations. One such potential start site would produce a truncated protein consisting of only zinc-finger domains. Moreover, if this protein was functional, the SB MO would be able to disrupt this transcript and protein, which could explain the HSC defect caused by the morpholino in the *snai2*$^{112\Delta}$ mutant embryos. However, studies have shown that *snai2* activity is largely dependent on the N-terminal SNAG and SLUG domains [54], so the truncated protein may not be sufficient to drive this function. Although protein analysis of Snail2 would be ideal to address these possibilities, testing of an available Snail2 antibody showed positive detection of murine, cardiac Snail2 was possible, but failed to detect zebrafish snail2 when overexpressed in HEK-293T cells (S8 Fig).

Finally, it is possible that the morpholino results in a dominant-negative protein which causes a negative effect on HSC specification. The misspliced transcript does not undergo nonsense mediated decay and accumulates, as shown by qPCR.

In summary, our results provide further evidence that understanding genetic function must be approached simultaneously with multiple approaches. The data presented here supports that the *snai2* morphant phenotype could be due to an off target or toxic event; however, this could also be due to reasons explained above, and further studies are necessary to deconvolute this problem.

Supporting information

S1 Fig. FACS and Morpholino controls. When double positive cells were sorted from *Tg (CD41*:*GFP/kdrl*:*mCherry)* embryos at 48 hpf, single positive mCherry only cells were also purified and qPCR performed with the same panel of genes: hematopoietic marker *cmyb*, endothelial marker *kdrl*, and *snai2* (A). As expected, *kdrl* was extremely elevated, while *cmyb* was decreased as compared to the rest of the embryo. *Snai2* is present, but extremely down regulated. Error bars are calculated from technical replicates. We confirmed efficacy of the SB MO by injecting into embryos and collecting a pool of embryos at 26 hpf. After RT-PCR was performed on a portion of the *snai2* transcript. 100% of the transcript appears to be the shortened length caused by the error in splicing (B).
(TIFF)

S2 Fig. Migration of the PLM and vascular cord formation is normal in SB morphants. WISH was performed on embryos injected with SB MO and their uninjected siblings to investigate migration of the PLM and formation of the vascular cord. We analyzed *fli1a*, a gene

actively expressed in the PLM as well as in the fully formed vasculature, as well as *kdrl*, a marker strong in the fully formed vasculature. At 14 and 18 hpf, *fli1a* staining showed normal formation of the PLM and timely migration to the midline (A). At 26 hpf, the vascular cord and caudal hematopoietic tissue appear largely normal by both *fli1a* and *kdrl* staining; however, the intersomitic vessels seem to have some trouble sprouting dorsally (B). Numbers in the lower right-hand corner of each image depict the number of embryos with the phenotype pictured out of the total number of embryos assayed in each condition.
(TIF)

S3 Fig. Primitive hematopoiesis and pronephros formation are unaffected in SB morphants. In order to observe other tissues involved in embryonic hematopoiesis, we assayed primitive hematopoiesis by WISH for the early erythroid marker *gata1* (A). SB morphants appeared to have normal primitive hematopoiesis initiation. We also observed formation of the pronephros, which will develop to be the adult HSC niche, by WISH for *cdh17* (B). Pronephric formation appeared normal in SB morphants. Numbers in the lower right-hand corner of each image depict the number of embryos with the phenotype pictured out of the total number of embryos assayed in each condition.
(TIF)

S4 Fig. Further analysis of ATG MO hematopoietic phenotype. ATG MO embryos were subjected to WISH for the hematopoietic marker *cmyb* at 48 hpf (A). The caudal hematopoietic tissue of morphant embryos showed a distinct reduction of *cmyb* staining as compared to their uninjected siblings. The morpholino was also injected into *Tg(CD41:GFP/kdrl:mCherry)* embryos and double positive fish were imaged via confocal microscopy at 48 hpf and Imaris imaging software was used to remove GFP signal outside of the vasculature (B). The surfaces feature of Imaris was utilized to quantify double positive cells (shown here in pink), and the resulting data was graphed and statistically analyzed by a non-parametric *t*-test on Prism (C). Error bars are SEM. There was a small, but significant decrease in the number of HSPCs in the ATG morphant fish. Numbers in the lower right-hand corner of each image depict the number of embryos with the phenotype pictured out of the total number of embryos assayed in each condition.
(TIFF)

S5 Fig. Further notch and somitic morphant data. In order to show not all Notch ligand expression was affected in *snai2* SB morphants, we analyzed aortic expression of *dll4* and *dlc* by WISH at 26 hpf (A). SB morphants showed normal levels of both ligands supporting that the aorta is specified correctly. The presence of the Notch intracellular domain in *Tg(UAS: NICD-myc)* embryos can be assayed by immunohistochemistry for the myc tag, fused to the NICD. Representative images were taken of positive and negative staining present when the transgenic was crossed to the *Tg(kdrl:miniGal4)* (B). Staining is visible in the dorsal aorta and caudal vein, as well as quite strongly in the caudal hematopoietic tissue of Gal4$^+$/NICD$^+$ embryos. Double fluorescent *in situ* for *dld* and *myoD* was performed in SB morphants and their siblings at 14 hpf, and the results imaged by confocal microscopy (C). Representative images show that morphant embryos have decreased somitic *dld* staining, especially within the more anterior somites. *myoD* in the same somites was expressed normally. We also analyzed *jam2a* expression by WISH (D), since not only is this gene expressed within the somites, but it has been shown to be essential for notch signal transduction to the migrating PLM. SB morphants showed normal expression of *jam2a*. Numbers in the lower right-hand corner of each image depict the number of embryos with the phenotype pictured out of the total number of embryos assayed in each condition.
(TIF)

S6 Fig. *Snai2*^{112Δ} **further analysis.** A representative gel image shows the different banding pattern observed when genotyping embryos from a *snai2*^{+/112Δ} in-cross (A). In order to assess later stages of embryonic hematopoiesis, we assessed expression of the T-cell marker, *rag1*, in 4 dpf embryos (B). Wild-types, heterozygotes, and mutants all showed normal *rag1* staining. When *snai2* mutants were analyzed on the *Tg(CD41:GFP/kdrl:mCherry)* background, we simultaneously injected a portion of the clutch analyzed with SB MO. These embryos were imaged via confocal microscopy and Imaris imaging software was used to remove GFP signal outside of the vasculature (C) alongside their uninjected siblings shown in Fig 7D. Quantification is shown in Fig 9D. Additionally, expression of the HSC specification marker, *runx1*, was analyzed by in situ hybridization at ~26 hpf in embryos injected with *snai2* ATG MO, *snai1a* morpholino (MO), and their siblings. Black arrowheads point to the middle of the aortic runx1 expression. Numbers in the lower right-hand corner of each image depict the number of embryos with the phenotype pictured out of the total number of embryos assayed in each condition.
(TIF)

S7 Fig. SB MO causes an increase in *p53* **transcript, but loss of** *p53* **does not rescue hematopoietic phenotype.** The potential of toxicity caused by the SB MO was analyzed by qPCR for *p53* in morphant and uninjected pooled embryos at 26 hpf (A). Via this analysis, we saw that indeed *p53* transcript was increased as compared to uninjected siblings. We also show *snai2* transcript levels, as they are consistently increased in SB MO injected embryos. SB MO was then injected into embryos derived from a *p53*^{+/-} in-cross, and the embryos analyzed for the hematopoietic markers *rag1* and *cmyb*. The loss of *p53* did not appear to rescue the morphant phenotype of decreased levels of both genes. Black arrowheads indicate the general position of the thymus.
(TIF)

S8 Fig. Western blot analysis shows available Snail2 antibody detects murine, but not zebrafish Snail2. Protein lysates from HEK-293T cells transfected with the zebrafish Snail proteins N-terminally tagged with green fluorescent protein (GFP) were analyzed via western blot for both GFP and Snail2. Mouse heart lysate was also run as a positive control for Snail2 presence. Protein size is indicated to the left of each blot. Lanes are labeled with the appropriate number representing the zebrafish Snail family member.
(TIFF)

Author Contributions

Conceptualization: Cara Bickers, Claire Pouget, David Traver.

Data curation: Cara Bickers, Sophia D. Española, Stephanie Grainger.

Formal analysis: Cara Bickers, Sophia D. Española, Claire Pouget.

Funding acquisition: David Traver.

Investigation: Cara Bickers, Sophia D. Española.

Methodology: Cara Bickers, Stephanie Grainger, Claire Pouget.

Project administration: David Traver.

Resources: Stephanie Grainger, David Traver.

Supervision: Claire Pouget, David Traver.

Writing ± original draft: Cara Bickers.

Writing ± review & editing: Cara Bickers, Sophia D. Española, Stephanie Grainger, David Traver.

References

1. Kissa K, Herbomel P. Blood stem cells emerge from aortic endothelium by a novel type of cell transition. Nature. 2010; 464: 112±115. https://doi.org/10.1038/nature08761 PMID: 20154732

2. Richard C, Drevon C, Canto PY, Villain G, Bollérot K, Lempereur A, et al. Endothelio-Mesenchymal Interaction Controls runx1 Expression and Modulates the notch Pathway to Initiate Aortic Hematopoiesis. Dev Cell. 2013; 24: 600±611. https://doi.org/10.1016/j.devcel.2013.02.011 PMID: 23537631

3. Bertrand JY, Chi NC, Santoso B, Teng S, Stainier DYR, Traver D. Haematopoietic stem cells derive directly from aortic endothelium during development. Nature. 2010; 464: 108±111. https://doi.org/10.1038/nature08738 PMID: 20154733

4. Boisset JC, Van Cappellen W, Andrieu-Soler C, Galjart N, Dzierzak E, Robin C. In vivo imaging of haematopoietic cells emerging from the mouse aortic endothelium. Nature. 2010; 464: 116±120. https://doi.org/10.1038/nature08764 PMID: 20154729

5. Jaffredo T, Gautier R, Eichmann A, Dieterlen-Lièvre F. Intraaortic Hemopoietic Cells Are Derived from Endothelial Cells During Ontogeny. Development. 1998; 125: 4575±4583. https://doi.org/10.1016/j.tcm.2006.02.005 PMID: 9778515

6. Swiers G, Rode C, Azzoni E, De Bruijn MFTR. A short history of hemogenic endothelium. Blood Cells, Mol Dis. 2013; 51: 206±212. https://doi.org/10.1016/j.bcmd.2013.09.005 PMID: 24095001

7. Kobayashi I, Kobayashi-Sun J, Kim AD, Pouget C, Fujita N, Suda T, et al. Jam1a-Jam2a interactions regulate haematopoietic stem cell fate through Notch signalling. Nature. 2014; 512: 319±323. https://doi.org/10.1038/nature13623 PMID: 25119047

8. Thompson M a., Ransom DG, Pratt SJ, MacLennan H, Kieran MW, Detrich HW, et al. The cloche and spadetail Genes Differentially Affect Hematopoiesis and Vasculogenesis. Dev Biol. 1998; 197: 248±269. https://doi.org/10.1006/dbio.1998.8887 PMID: 9630750

9. Grainger S, Richter J, Palazón RE, Pouget C, Lonquich B, Wirth S, et al. Wnt9a Is Required for the Aortic Amplification of Nascent Hematopoietic Stem Cells. Cell Rep. 2016; 17: 1595±1606. https://doi.org/10.1016/j.celrep.2016.10.027 PMID: 27806298

10. Clements WK, Kim AD, Ong KG, Moore JC, Lawson ND, Traver D. A somitic Wnt16/Notch pathway specifies haematopoietic stem cells. Nature. 2011; 474: 220±225. https://doi.org/10.1038/nature10107 PMID: 21654806

11. Kim AD, Melick CH, Clements WK, Stachura DL, Distel M, Panáková D, et al. Discrete Notch signaling requirements in the specification of hematopoietic stem cells. Embo J. 2014; 33: 2363±2374. https://doi.org/10.15252/embj.201488784 PMID: 25230933

12. Lee Y, Manegold JE, Kim AD, Pouget C, Stachura DL, Clements WK, et al. FGF signalling specifies haematopoietic stem cells through its regulation of somitic Notch signalling. Nat Commun. 2014; 5: 1±13. https://doi.org/10.1038/ncomms6583 PMID: 25428693

13. Nguyen PD, Hollway GE, Sonntag C, Miles LB, Hall TE, Berger S, et al. Haematopoietic stem cell induction by somite-derived endothelial cells controlled by meox1. Nature. 2014; 512: 314±318. https://doi.org/10.1038/nature13678 PMID: 25119043

14. Wagers AJ. The stem cell niche in regenerative medicine. Cell Stem Cell. Elsevier Inc.; 2012; 10: 362±369. https://doi.org/10.1016/j.stem.2012.02.018 PMID: 22482502

15. Charbord P, Pouget C, Binder H, Dumont F, Stik G, Levy P, et al. A systems biology approach for defining the molecular framework of the hematopoietic stem cell Niche. Cell Stem Cell. 2014; 15: 376±391. https://doi.org/10.1016/j.stem.2014.06.005 PMID: 25042701

16. Manzanares M, Locascio A, Nieto MA. The increasing complexity of the Snail gene superfamily in metazoan evolution. Trends Genet. 2001; 17: 178±181. https://doi.org/10.1016/S0168-9525(01)02232-6 PMID: 11275308

17. Nieto MA. The snail superfamily of zinc-finger transcription factors. Nat Rev Mol Cell Biol. 2002; 3: 155±166. https://doi.org/10.1038/nrm757 PMID: 11994736

18. Yang J, Weinberg RA. Epithelial-Mesenchymal Transition: At the Crossroads of Development and Tumor Metastasis. Dev Cell. 2008; 14: 818±829. https://doi.org/10.1016/j.devcel.2008.05.009 PMID: 18539112

19. Strobl-Mazzulla PH, Bronner ME. A PHD12-Snail2 repressive complex epigenetically mediates neural crest epithelial-to-mesenchymal transition. J Cell Biol. 2012; 198: 999±1010. https://doi.org/10.1083/jcb.201203098 PMID: 22986495

20. Inoue A, Seidel MG, Wu W, Kamizono S, Ferrando AA, Bronson RT, et al. Slug, a highly conserved zinc finger transcriptional repressor, protects hematopoietic progenitor cells from radiation-induced apoptosis in vivo. Cancer Cell. 2002; 2: 279±288. https://doi.org/10.1016/S1535-6108(02)00155-1 PMID: 12398892

21. Sun Y, Shao L, Bai H, Wang ZZ, Wu W-S. Slug deficiency enhances self-renewal of hematopoietic stem cells during hematopoietic regeneration. Blood. 2010; 115: 1709±1717. https://doi.org/10.1182/blood-2009-07-232934 PMID: 20032500

22. Pérez-Losada J, Sánchez-Martín M, Rodríguez-García A, Sánchez ML, Orfao A, Flores T, et al. Zinc-finger transcription factor Slug contributes to the function of the stem cell factor c-kit signaling pathway. Blood. 2002; 100: 1274±1286. PMID: 12149208

23. Pioli PD, Dahlem TJ, Weis JJ, Weis JH. Deletion of Snai2 and Snai3 Results in Impaired Physical Development Compounded by Lymphocyte Deficiency. PLoS One. 2013; 8: 1±19. https://doi.org/10.1371/journal.pone.0069216 PMID: 23874916

24. Pioli PD, Chen X, Weis JJ, Weis JH. Fatal autoimmunity results from the conditional deletion of Snai2 and Snai3. Cell Immunol. 2015; 295: 1±18. https://doi.org/10.1016/j.cellimm.2015.02.009 PMID: 25732600

25. Novodvorsky P, Watson O, Gray C, Wilkinson RN, Reeve S, Smythe C, et al. Klf2ash317mutant zebrafish do not recapitulate morpholino-induced vascular and haematopoietic phenotypes. PLoS One. 2015; 10. https://doi.org/10.1371/journal.pone.0141611 PMID: 26506092

26. Eve AMJ, Place ES, Smith JC. Comparison of Zebrafish tmem88a mutant and morpholino knockdown phenotypes. PLoS One. 2017; 12: 1±17. https://doi.org/10.1371/journal.pone.0172227 PMID: 28192479

27. Place ES, Smith JC. Zebrafish atoh8 mutants do not recapitulate morpholino phenotypes. PLoS One. 2017; 12: 1±12. https://doi.org/10.1371/journal.pone.0171143 PMID: 28182631

28. Kok FO, Shin M, Ni CW, Gupta A, Grosse AS, VanImpel A, et al. Reverse genetic screening reveals poor correlation between morpholino-induced and mutant phenotypes in zebrafish. Dev Cell. 2015; 32: 97±108. https://doi.org/10.1016/j.devcel.2014.11.018 PMID: 25533206

29. Law SHW, Sargent TD. The serine-threonine protein kinase PAK4 is dispensable in zebrafish: Identification of a morpholino-generated pseudophenotype. PLoS One. 2014; 9. https://doi.org/10.1371/journal.pone.0100268 PMID: 24945275

30. Stainier DYR, Raz E, Lawson ND, Ekker SC, Burdine RD, Eisen JS, et al. Guidelines for morpholino use in zebrafish. PLoS Genet. 2017; 13: 6±10. https://doi.org/10.1371/journal.pgen.1007000 PMID: 29049395

31. Westerfield M. The Zebrafish Book. A Guide for the Laboratory Use of Zebrafish (Danio rerio), 5th Edition. 2007.

32. Lin HF, Traver D, Zhu H, Dooley K, Paw BH, Zon LI, et al. Analysis of thrombocyte development in CD41-GFP transgenic zebrafish. Blood. 2005; 106: 3803±3810. https://doi.org/10.1182/blood-2005-01-0179 PMID: 16099879

33. Chi NC, Shaw RM, Val S De, Kang G, Jan LY, Black BL, et al. Foxn4 directly regulates tbx2b expression and atrioventricular canal formation. Genes Dev. 2008; 22: 734±739. https://doi.org/10.1101/gad.1629408 PMID: 18347092

34. Butko E, Distel M, Pouget C, Weijts B, Kobayashi I, Ng K, et al. Gata2b is a restricted early regulator of hemogenic endothelium in the zebrafish embryo. Development. 2015; 142: 1050±1061. https://doi.org/10.1242/dev.119180 PMID: 25758220

35. Higashijima SI, Okamoto H, Ueno N, Hotta Y, Eguchi G. High-frequency generation of transgenic zebrafish which reliably express GFP in whole muscles or the whole body by using promoters of zebrafish origin. Dev Biol. 1997; 192: 289±299. PMID: 9441668

36. Parsons MJ, Pisharath H, Yusuff S, Moore JC, Siekmann AF, Lawson N, et al. Notch-responsive cells initiate the secondary transition in larval zebrafish pancreas. Mech Dev. 2009; 126: 898±912. https://doi.org/10.1016/j.mod.2009.07.002 PMID: 19595765

37. Scheer N, Campos-Ortega JA. Use of the Gal4-UAS technique for targeted gene expression in the zebrafish. Mech Dev. 1999; 80: 153±158. https://doi.org/10.1016/S0925-4773(98)00209-3 PMID: 10072782

38. Busch-Nentwich E, Kettleborough R, Dooley CM, Scahill C, Sealy I, White R, et al. Sanger Institute Zebrafish Mutation Project mutant data submission, ZFIN Direct Data Submission [Internet]. 2013. Available: http://zfin.org

39. Berghmans S, Murphey RD, Wienholds E, Neuberg D, Kutok JL, Fletcher CDM, et al. Tp53 Mutant Zebrafish Develop Malignant Peripheral Nerve Sheath Tumors. Proc Natl Acad Sci. 2005; 102: 407±412. https://doi.org/10.1073/pnas.0406252102 PMID: 15630097

40. Montague TG, Cruz JM, Gagnon JA, Church GM, Valen E. CHOPCHOP: A CRISPR/Cas9 and TALEN web tool for genome editing. Nucleic Acids Res. 2014; 42: 401±407. https://doi.org/10.1093/nar/gku410 PMID: 24861617

41. Labun K, Montague TG, Gagnon JA, Thyme SB, Valen E. CHOPCHOP v2: a web tool for the next generation of CRISPR genome engineering. Nucleic Acids Res. 2016; 44: W272±W276. https://doi.org/10.1093/nar/gkw398 PMID: 27185894

42. Gagnon JA, Valen E, Thyme SB, Huang P, Ahkmetova L, Pauli A, et al. Efficient mutagenesis by Cas9 protein-mediated oligonucleotide insertion and large-scale assessment of single-guide RNAs. PLoS One. 2014; 9: 5±12. https://doi.org/10.1371/journal.pone.0098186 PMID: 24873830

43. Brend T, Holley SA. Zebrafish Whole Mount High-Resolution Double Fluorescent In Situ Hybridization. J Vis Exp. 2009; 5±9. https://doi.org/10.3791/1229 PMID: 19322135

44. Shestopalov IA, Pitt CLW, Chen JK. Spatiotemporal resolution of the Ntla transcriptome in axial mesoderm development. Nat Chem Biol. 2012; 8: 270±276. https://doi.org/10.1038/nchembio.772 PMID: 22286130

45. Bertrand JY, Cisson JL, Stachura DL, Traver D. Notch signaling distinguishes 2 waves of definitive hematopoiesis in the zebrafish embryo. Blood. 2010; 115: 2777±2783. https://doi.org/10.1182/blood-2009-09-244590 PMID: 20107232

46. Nusslein-Volhard C, Dahm R. Zebrafish: a practical approach. New York: Oxford University Press;

47. Ye S, Dhillon S, Ke X, Collins AR, Day INM. An efficient procedure for genotyping single nucleotide polymorphisms. Nucleic Acids Res. 2001; 29: e88±e88. https://doi.org/10.1093/nar/29.17.e88 PMID: 11522844

48. Stachura DL, Reyes JR, Bartunek P, Paw BH, Zon LI, Traver D. Zebrafish kidney stromal cell lines support multilineage hematopoiesis. Blood. 2009; 114: 279±289. https://doi.org/10.1182/blood-2009-02-203638 PMID: 19433857

49. Traver D, Paw BH, Poss KD, Penberthy WT, Lin S, Zon LI. Transplantation and in vivo imaging of multilineage engraftment in zebrafish bloodless mutants. Nat Immunol. 2003; 4: 1238±1246. https://doi.org/10.1038/ni1007 PMID: 14608381

50. Butko E, Pouget C, Traver D. Complex regulation of HSC emergence by the Notch signaling pathway. Dev Biol. 2016; 409: 129±138. https://doi.org/10.1016/j.ydbio.2015.11.008 PMID: 26586199

51. Rossi A, Kontarakis Z, Gerri C, Nolte H, Hölper S, Krüger M, et al. Genetic compensation induced by deleterious mutations but not gene knockdowns. Nature. 2015; 524: 230±233. https://doi.org/10.1038/nature14580 PMID: 26168398

52. Robu ME, Larson JD, Nasevicius A, Beiraghi S, Brenner C, Farber SA, et al. P53 Activation By Knockdown Technologies. PLoS Genet. 2007; 3: 787±801. https://doi.org/10.1371/journal.pgen.0030078 PMID: 17530925

53. Su CY, Kemp HA, Moens CB. Cerebellar development in the absence of Gbx function in zebrafish. Dev Biol. 2014; 386: 181±190. https://doi.org/10.1016/j.ydbio.2013.10.026 PMID: 24183937

54. Molina-Ortiz P, Villarejo A, MacPherson M, Santos V, Montes A, Souchelnytskyi S, et al. Characterization of the SNAG and SLUG domains of Snail2 in the repression of E-cadherin and EMT induction: Modulation by serine 4 phosphorylation. PLoS One. 2012; 7: 1±12. https://doi.org/10.1371/journal.pone.0036132 PMID: 22567133